MODELLING OF MATERIAL PHENOMENA OF STEEL IN CONSTITUTIVE RELATIONS IN CONTEXT OF WELDING

I. Wudtke[*]

[*]*Bauhaus-Universität Weimar, Research Training Group 1462
Berkaer Str. 9, 99 423 Weimar, Germany*
E-mail: idna.wudtke@uni-weimar.de

Keywords: steel, welded connections, metallurgical transformation, residual stress

Abstract. *The alteration of metallurgical constitution of the weld and the heat-affected zone (HAZ), in comparison to the base material, as well as appearance of residual stress and distortion in the welded connection are the major effects due to welding. The goal of this paper is to describe the constitutive relations which must be taken into consideration when predicting the welding results, as well as to show the wide range of material properties which influence the calculated responses. Therefore the thermal, metallurgical and mechanical behaviors of steel have to be considered. The time dependent temperature distribution during heating and cooling is dependent on the heat impact of the heat source as well as the heat accumulation, conductivity and heat loss due to radiation and convection effects. The metallurgical transformation in the weld and the heat-affected zone is strongly effected by the non-linear temperature rate. The presented Leblond-Model describes transformation kinetics in the material considering diffusion and diffusionless controlled transformations due to the discontinious heating and cooling rates. Furthermore applying this model, it is possible to consider the grain size effect with respect to the transformation kinetics. The mechanical phenomena needed for the calculation of the residual stress distribution and distortion of the workpiece are also presented. Material properties are discussed regarding the practicability of their experimental identification. Considering the described thermal and metallurgical phenomena, the results of a numerical simulation of a welded butt joint of the fine grained high strength steel, S460M, are shown and compared with experimental data. To consider or neglect the metallurgical phenomena during heating and cooling process will cause significantly different numerical results for the residual stress distribution.*

1 INTRODUCTION

Design and quality of welded connections are inherent to the responsibility of structural and quality management engineers within the field of structural steel engineering. Despite the fact that the prediction of quality of the joints can influence the design parameters, in reality these two disciplines are mostly disconnected from each other. The application of partly decoupled approach by means of continuum mechanics facilitates the calculation of structural responses due to welding with FEM. The numerical results demonstrate the ability of a qualitative prediction of welded connections. As it is intended to integrate the local effects of a joint in structural analysis of steel constructions, it is necessary to meet higher approaches towards quality. The microstructure of material in the weld and the heat-affected zone (HAZ) changes. This change results an alteration of mechanical properties in the local areas due to high thermal impact during welding. Thus, residual stresses and distortion affect the deformation and bearing capacity of welded constructions. The numerical simulation of the welding process by finite element analysis is state of the art for the deduction of described local effects. Therefore a description of thermal, metallurgical and mechanical behavior as well as of their complex interactions is necessary. Since the phenomena, which characterize the material behavior, depend on a large amount of material parameters as well as initial and boundary conditions, the calculated results have to be seen as a deductive approach. Furthermore this approach has to be analyzed keeping in mind the practicability of parameter identification and their influence on the calculated responses.

2 THERMAL BEHAVIOR

2.1 Practical Requirements

For the analysis of welds, it is necessary to calculate the temperature distribution in the connection depending on time. It is imperative to describe the heat impact on the workpiece due to welding and the thermal behavior of the material. As it is of vital importance to the resulting microstructural transformation and thermal strain within the workpiece, there is an emphasis on the calculated heat volume and fluctuating heating and cooling rates. One of the challenges is to describe the thermal behavior of the workpiece by ignoring the explicit description of fluid dynamics in the molten weld pool. The surrounding conditions during manufacturing can also greatly influence the temperature distribution and rate. Therefore these influences have to be considered.

2.2 Theoretical Background and Description of Parameters

Numerical calculation of thermal processes is relies on the formulation of energy equilibrium state principles. Therefore it is assumed that the energy balance follows the equation:

$$\delta \dot{Q}_i - \delta \dot{Q}_s - \delta \dot{Q}_b = 0 \tag{1}$$

This balance can be set up for any system implying the amount of the heat flux change of respectively the total amount of incoming heat flux $\delta \dot{Q}_i$, the total amount of outgoing heat flux $\delta \dot{Q}_s$ and the total amount of accumulated heat flux $\delta \dot{Q}_b$.

Based on Fourier's heating law, an energy balance is drawn according to 1st fundamental theorem of thermodynamics to signify the equilibrium state according to [[3]]:

$$\rho c_p \frac{\delta \theta}{\delta t} = div \left[\lambda \cdot grad\theta \right] + \dot{Q}_b \left(x, y, z, t \right) \tag{2}$$

Thus it is possible to calculate the transient distribution of temperature θ depending on arising heat flux $\dot{Q}_b$ within the workpiece. Material behavior is integrated by means of temperature dependent material parameters: density - $\rho \left[\frac{kg}{m^3} \right]$, specific heat capacity - $c_p \left[\frac{J}{kg \cdot K} \right]$ and specific heat conductivity - $\lambda \left[\frac{W}{K \cdot m} \right]$. During the heating and cooling processes a metallurgical transformation and change of aggregate state occurs. The energy needed for the transformation leads to an increasing amount of accumulated thermal energy within the workpiece (Gibbs free enthalpy). This effect can be taken into account by applying a discontinuous specific enthalpy function as shown in the figure 1.
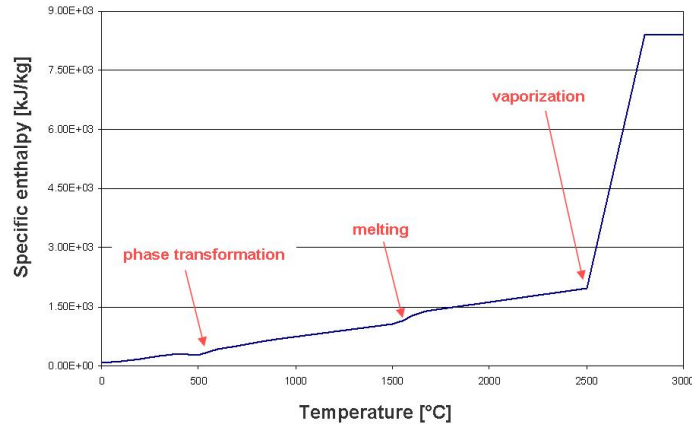

Figure 1: Specific enthalpy (acc. to [4])

The specific enthalpy - $h \left[\frac{J}{kg} \right]$, represents the temperature dependent amount of internal energy within the system:

$$h \left(\theta \right) = \int_{\theta_0}^{\theta} c_p \, d\theta \tag{3}$$

Several laborious methods have to be carried out for the experimental determination of thermal material parameters. As it is of utmost importance all parameters have to be measured depending on temperature.

To determine the density function a buoyancy-flotation method at room temperature has to be carried out. Assuming constant mass and isotropic thermal strain, the dependence of density on the temperature can be calculated by means of the coefficient of thermal expansion [5]. The density of steel materials decreases proportionally with increasing temperature.

The heat and the heat flux can be measured by means of differential scanning calorimetry (DSC) [5]. Dispositive heat flux difference between the oven and the sample specimen as well as the oven and the reference specimen during a defined temperature-time process gives information about enthalpy and specific heat capacity of the material.

It is possible to indirectly identify specific heat conductivity experimentally by applying the laser flash method (LFM) on a specimen in an oven at steady temperature states [5]. Highly sensitive detectors measure the increasing temperature against the time due to the laser flash. Thus the thermal conductivity - $a \left[\frac{m^2}{s} \right]$, can be identified. The specific heat conductivity can be calculated subsequently based on density, specific heat capacity and thermal conductivity, as shown in equation 4. The information about every thermal material property is required as a function of temperature.

$$\lambda \left(\theta \right) = c_p \left(\theta \right) \cdot \rho \left(\theta \right) \cdot a \left(\theta \right) \tag{4}$$

As there are numerous different welding treatments, the specific characteristic of the utilized process has to be represented within the mathematical formulation of the heat source. The double ellipsoidal heat source with normal distribution according to Goldak enables the formulation of thermal impact on the workpiece due to metal-active-gas welding (MAG):

$$Q_i = \int_V q_{eff} \cdot e^{-AFx^2 - By^2 - Cz^2} \, dV + \int_V q_{eff} \cdot e^{-ARx^2 - By^2 - Cz^2} \, dV \tag{5}$$

The geometric parameters AF, AR, B and C have to be adapted by means of developing molten pool geometry. The motion of the arc during welding is represented by different normal distributions in front and behind the yz-plane (see figure 2).
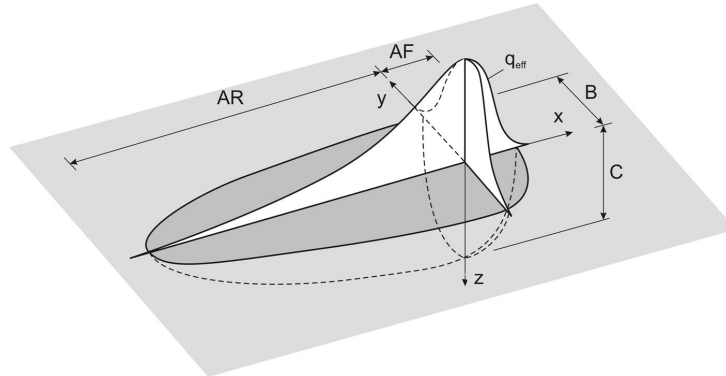

Figure 2: Heat source according to Goldak [11]

The heat source according to Goldak enables the application of a 3D thermal loading on the workpiece sufficiently. However, the loading influence ends at the position where heat flux is equal to 5% of effective heat flow density. The effective heat flow density is describing the incoming amount of energy into the system being transformed from electric energy to thermal energy within the MAG welding. This value quantifies the welding process as it obeys the following equation:

$$q_{eff} = U_W \cdot I_W \cdot \eta_W \tag{6}$$

The process parameters: welding voltage - U_W $[V]$, welding current - I_W $[A]$ and the efficiency factor η_W are directly influencing the thermal load on the workpiece according to equation (5). The efficiency factor represents the heat loss due to spraying and vaporization during welding. In the literature factor of 0.8 is recommended when simulating the MAG welding process [6]. The heat source is moving along the workpiece at the welding velocity - v_W $\left[\frac{m}{s} \right]$.

2.3 Boundary Conditions

During heating and cooling a heat transmission between the welded workpiece and the surrounding media occurs. This influences the temperature distribution within the workpiece. There are two phenomena which describe this effect in a sufficient manner - convection and radiation. The induced heat loss on bordering surfaces due to convection and radiation which can be expressed by Newton's law of cooling:

$$\delta \dot{Q}_s = \alpha \cdot (\theta_W - \theta_A) \tag{7}$$

The equation shows that the heat volume rate outgoing from the workpiece is proportional to the temperature differences between the body θ_W and its environment θ_A. The factor of proportion is a heat transfer coefficient - $\alpha \left[\frac{W}{m^2 \cdot K} \right]$, which can be expressed as a sum of coefficients describing the convenction and radiation:

$$\alpha = \alpha_C - \alpha_R \tag{8}$$

Convective and radiative heat transfers clearly differ from each other. As there is no proof of the interaction of these two phenomena, their coefficients can be identified separately [4].

Convective heat loss occurs due to heat conduction (natural convection) and transmission of thermal energy by flow motion (forced convection) of the surrounding media. Thus, ambient conditions during manufacturing, i.e. wind during outdoor welding, latent air in the factory hall or underwater welding, can be taken into account considering the forced convection phenomenon. To determine the convective heat transfer coefficient, numerous phenomenological and empirical relations have to be considered describing the constitution of surrounding media and its behavior as described in [4] and [8].

Radiative heat transfer takes place in the form of electromagnetic waves. In contrast to convective heat transfer the radiative heat transfer is not conditional on the surrounding media. It is, on the other side, highly depending on the material of the welded workpiece, its surface condition, the temperature and the direction of radiation. The amount of radiation emitted from a body can be experimentally determined by means of infrared thermography, with respect to measured results of a black body [7]. Convective and radiative heat transfer coefficients have to be identified as functions depending on temperature.

As there is a variety of parameters influencing the coefficients of convective and radiative heat transfer, the experimental complexity rises disproportionately. For that reason a presumption using table values from literature is recommended and mostly used. Table 1 shows a summary of thermal material parameters including parameters for the definition of boundary conditions.

material parameter	unit	identification
density - ρ	$\frac{kg}{m^3}$	buoyancy-flotation & dilatometry, indirect method
specific enthalpy - h	$\frac{J}{kg}$	DSC, direct method
specific heat capacity - c_p	$\frac{J}{kg \cdot K}$	DSC, indirect method
specific thermal conductivity - a	$\frac{m^2}{s}$	dilatometry & CCT, indirect method
specific heat conductivity - λ	$\frac{W}{K \cdot m}$	LFM, indirect method
convective heat transfer coefficient - α_C	$\frac{W}{m^2 \cdot K}$	LFM & other, indirect method
radiative heat transfer coefficient - α_R	$\frac{W}{m^2 \cdot K}$	infrared thermography, indirect method

Table 1: Overview of thermal material parameters

3 METALLURGICAL BEHAVIOR

3.1 Metallurgical Phenomena Due to Welding

Due to high thermal impact a metallurgical transformation of steel microstructure in the weld and the HAZ occurs. The transformation behavior of a steel depends on its initial microstructural state, chemical composition, the temperature and the rate of the temperature change in the workpiece. The different crystal lattice dimensions of microstructural phases cause local volume changes during the transformation process. Thus, this phenomenon influences the mechanical behavior of the welded connection. Besides that, the mechanical properties of microstructural phases of steel are different. Due to the fact that the temperature and the rate of the temperature change during welding in the workpiece are non-linear, the microstructural evolution has to be described for different thermal histories. A slow cooling process enables a complete diffusion of alloys during the microstructural transformation causing development of phases in an equilibrium state (i.e. ferrite phase). Whereas a high cooling rate induces a diffusionless transformation resulting in an unbalanced metallurgical state (i.e. martensitic phase). Therefore the diffusion and diffusionless controlled transformations have to be taken into account. Required information is the local phase volume proportions during the heating and the cooling process.

3.2 Leblond-Model

Phase transformation is a microscopic mechanism which is influencing the macroscopic behavior of the material. In order to determine phase volume fractions in weld and HAZ during heating and cooling of a welding process, several models have been developed for the description of the transformation behavior depending on temperature-time regime. Leblond-Model is a semi-empirical model, well suited to characterize the transformation behavior. This approach obeys the assumption that, during a transformation from phase j to phase i, the phase i can reach its temperature dependent equilibrium state - $p_{i,eq}^{ji}(\theta)$. The transformation kinetic is dependent on reaction inertia - $\tau_{ji}(\theta)$ and on temperature rate which is represented by a function - $f_{ji}(\dot{\theta})$. Figure 3 illustrates the athermal transformation to a phase i as a hysteresis loop. Depending on a thermal regime, phase i can have different phase volume proportions in an equilibrium state.
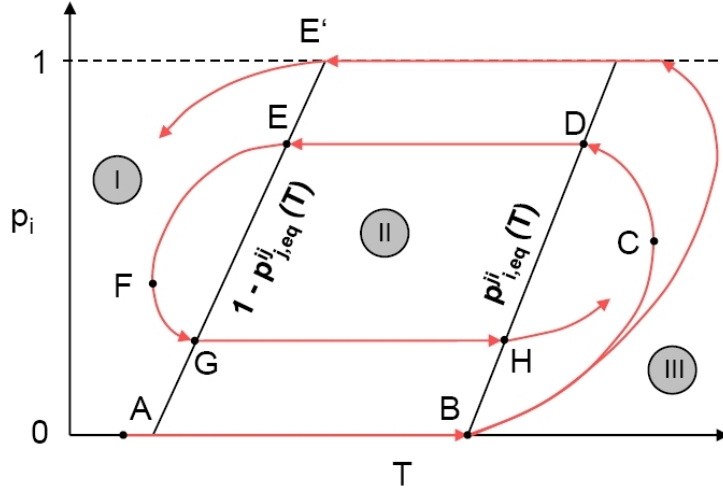
6

Figure 3: Athermal phase transformation of Leblond-Model acc. to [11]

The transformation between n different phases can be expressed according to [10] as follows:

$$\frac{dp_i\left(\theta,\,\dot{\theta},\,t\right)}{dt} = \dot{p}_i\left(\theta\right) = -\sum_{j\neq i} A_{ij} \quad (i = 1,\,2,\,...,\,n) \tag{9}$$

with

$$A_{ij} = \begin{cases} \underbrace{\left(-\dfrac{p_{j,eq}^{ij}\left(\theta\right)}{\tau^{ij}\left(\theta\right)}p_i\left(\theta,t\right) + \dfrac{1 - p_{j,eq}^{ij}\left(\theta\right)}{\tau^{ij}\left(\theta\right)}p_j\left(\theta,t\right)\right)f_{ij}\left(\dot{\theta}\right)}_{l_{ij}} & \forall\,l_{ij} > 0 \quad (i \longrightarrow j)\,; \\[3em] \underbrace{\left(-\dfrac{p_{i,eq}^{ji}\left(\theta\right)}{\tau^{ji}\left(\theta\right)}p_j\left(\theta,t\right) + \dfrac{1 - p_{i,eq}^{ji}\left(\theta\right)}{\tau^{ji}\left(\theta\right)}p_i\left(\theta,t\right)\right)f_{ji}\left(\dot{\theta}\right)}_{l_{ji}} & \forall\,l_{ji} > 0 \quad (j \longrightarrow i)\,; \\[3em] 0 & \forall\,l_{ij} \leq 0 \,\wedge\, l_{ji} \leq 0. \end{cases} \tag{10}$$

Furthermore, the austenite grain size is influencing the transformation behavior by affecting the transformation speed. This phenomena can be taken into account devising the change of grain size - D depending on the activation energy - Q, nucleation constant - C, gas constant - R and temperature - T with an exponent - a, assuming the following relation according to [10]:

$$\frac{dD^a}{dt} = C\,e^{\left(-\frac{Q}{RT}\right)} \tag{11}$$

The interconnection of the semi-empirical evolution equations (11) with (9) and (10) forms a system of differential equations for modeling the transformation kinetics by Leblond-Model. The detailed approach is described in [11]. Leblond-Model enables the consideration of diffusion controlled and diffusionless transformation processes.

3.3 Description of Parameters

Material properties characterizing the metallurgical behavior in Leblond-Model are equilibrium state proportions $p^{ij}_{j,eq}, p^{ji}_{i,eq}$, reaction inertia functions τ^{ij}, τ^{ji} and temperature rate functions f_{ij}, f_{ji} due to transformation between phases i and j. They can be specified in a continuous cooling transformation diagram, CCT, which is expressing the extent of transformation as a function of time for a continuously decreasing temperature, measured by dilatometry. A large number of experiments is required to build up a complete CCT-diagram 4. As the transformation behavior is strongly depending on chemical composition, a CCT-diagram is representative only for the tested steel material.
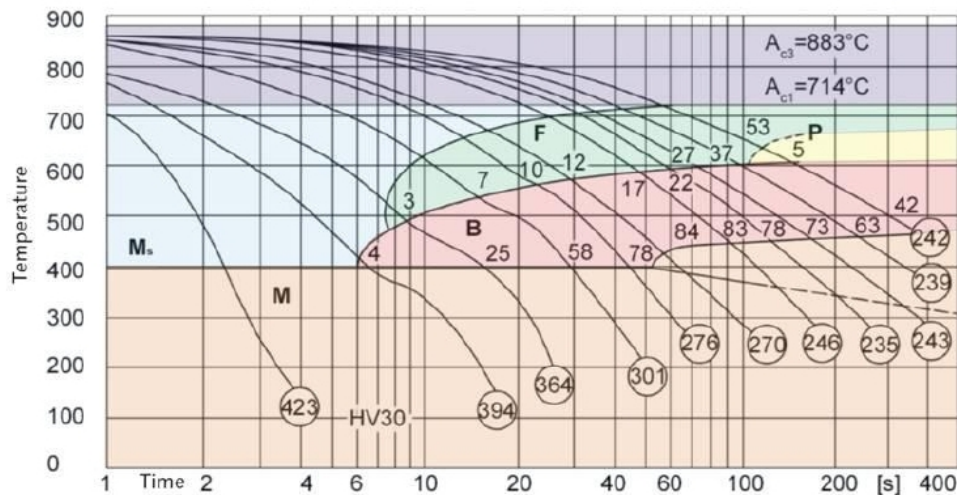

Figure 4: Continuous cooling transformation diagram of S460M

There are numerous methods for measurement of the grain size. The most common, planimetric method yields the number of grains per square millimeter area on a microsection from which it is possible to calculate the average grain area. The square root of average grain area is presenting the grain diameter D. Equivalent approaches for measuring grain size using tablet digitizer systems and fully automatic systems are possible. The nucleation constant C can be experimentally identified by means of petrographic microscopy, observing the process of austenitization by different temperature rates.

The complexity of metallurgical transformation phenomena requires the quantification of a high variety of microscopic material parameters. For the prediction of phase proportions in the welded connection, the CCT-diagram of the steel grade with identical chemical composition is unconditional.

Table 2 shows an overview of material parameters required for the description of metallurgical transformation kinetics of welded steel material.

material parameter	unit	identification
phase proportions equilibrium state - $p_{j,eq}^{ij}, p_{i,eq}^{ji}$	$[-]$	dilatometry & CCT, indirect method
reaction inertia functions - τ^{ij}, τ^{ji}	$\left[\frac{1}{s}\right]$	dilatometry & CCT, indirect method
temperature rate functions - f_{ij}, f_{ji}	$\left[\frac{K}{s}\right]$	dilatometry & CCT, indirect method
austenite grain size - D	$[nm]$	microsection, indirect method
nucleation constant - C	$[-]$	petrographic microscopy, indirect method

Table 2: Overview of metallurgical material parameters

4 MECHANICAL BEHAVIOR

4.1 Theoretical Background and Description of Parameters

For the determination of residual stresses and distortion state after welding, the description of mechanical behavior is necessary. During heating and cooling processes, strains due to different phenomena occur locally, interacting with each other, resulting in a residual stress or distortion state after cooling, due to existence of mechanical and material constraints. The macroscopic constitutive equation that describes the mechanical behavior of material undergoing the metallurgical transformation is generally expressed by assuming the total strain as a sum of different strain phenomena:

$$\epsilon_{ij} = \epsilon_{ij}^{el} + \epsilon_{ij}^{th} + \epsilon_{ij}^{tp} + \epsilon_{ij}^{pl} \tag{12}$$

ϵ_{ij}^{el} is the elastic strain state which is related to the stress state σ_{ij} by Hook's law. Assuming an isotropic material behavior, Young's modulus E and Poisson's ratio ν have to be expressed depending on temperature and microstructure, following the equation:

$$\epsilon_{ij}^{el} = \frac{(1 + \nu)\,\sigma_{ij} - \delta_{ij}\nu\sigma_m}{E} \tag{13}$$

In the equation (13), σ_m is representing the mean stress and δ_{ij} the Kroneckers delta.

ϵ_{ij}^{th} is the thermal strain due to thermal expansion of different phases and their dependence on temperature. It implies the strain associated with the microstructural transformations. The amount of transformation induced strain is not equal during heating and cooling, as shown in figure 5. It is assumed that the total amount of thermal strain can be described decomposed as a sum of thermal strains of each of transforming phases i and j (see eq. (14)). Furthermore, the thermal strain of a metallurgical phase i can be expressed as a product of thermal coefficient of expansion - α_i^{th} and temperature change - $\delta\theta$; as shown in the following equation:

$$\epsilon^{th} = p_i\epsilon_i^{th} + p_j\epsilon_j^{th} \ \wedge \ \epsilon^{th} = \alpha^{th}\,\delta\theta \tag{14}$$
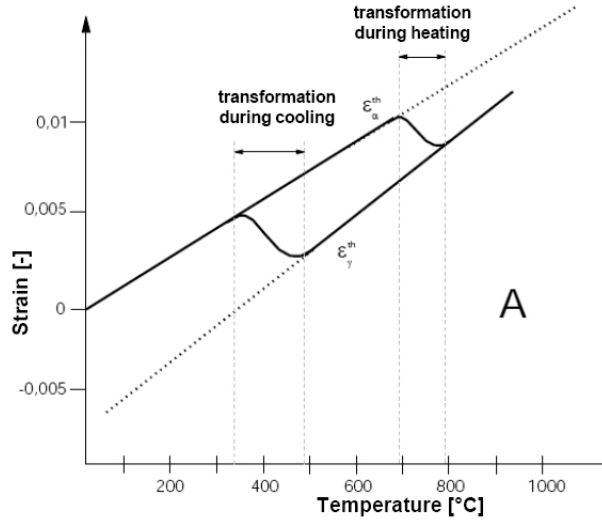
Figure 5: Thermal strains including effects of microstructural transformation [11]

Another considered phase transformation induced phenomenon is the transformation plasticity.
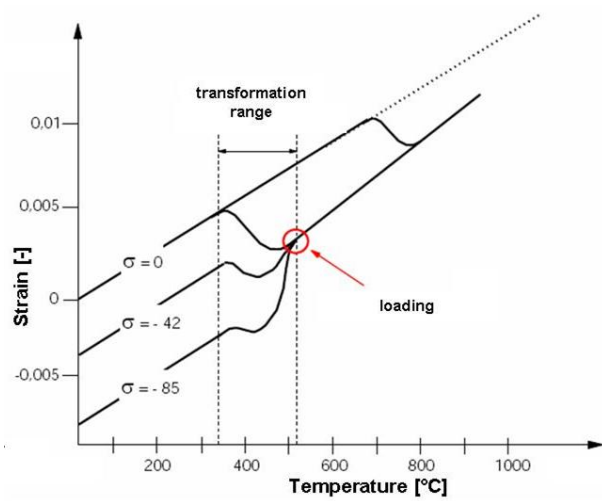

Figure 6: Transformation plasticity during dilatometry under loading conditions [11]

Figure 6 demonstrates the developing of strain due to metallurgical transformation under mechanical loading. The induced strain causes plastic deformations, even though the yield strength of material is not reached. The amount of plastic strain - ϵ_{ij}^{tp} caused by this effect can be described by Leblond's modification of Greenwood-Johnson-Model, defined according to [13] as follows:

$$\epsilon_{ij}^{tp} = 3\Delta\epsilon_{i\rightarrow j}^{th} S \int_{t_1}^{t_0} \frac{1}{f_{y,p_i}} ln\left(p_i\right) \dot{p}_i \, dt \tag{15}$$

10

The Greenwood-Johnson-Model is describing the amount of plastic strain that is influenced by the thermal strain difference between phases i and j during their transformation - $\Delta\epsilon_{i\to j}^{th}$. Furthermore the phase proportion of a weakest phase - p_i, as well as its transformation fraction rate - $\dot{p}_i$ and its yield strength - f_{y,p_i} are affecting the development of this phenomenon. The phase proportion as well as its fraction rate can be calculated by means of Leblond-Model, described in 3.2.

The description of plastic material behavior is implemented by means of von Mises yield criterion and plastic evolution law considering the kinematic hardening effect. Von Mises yield criterion defines the crossing between the elastic and plastic material behavior comparing the equivalent stress - σ_v with the yield stress - f_y. According to [2], the function of the yield surface - $f(\sigma)$ can be assumed as in equation (16). The application of von Mises yield criterion implies that the yielding occur due to deviatoric stress components, represented by deviatoric stress tensor - s_{ij}, by neglecting hydrostatic stress component:

$$f(\sigma) = \sqrt{s_{ij}s_{ij}} - \sqrt{\frac{2}{3}}f_y \tag{16}$$

The plastic material behavior is assumed, applying kinematic hardening effect as illustrated in the figure 7.
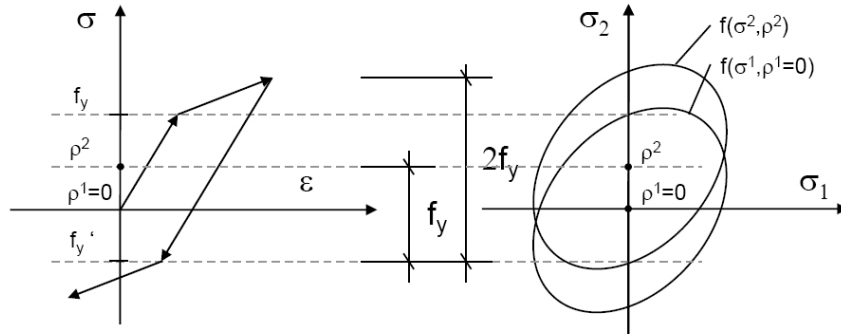

Figure 7: Kinematic hardening effect [2]

The kinematic hardening presumes a transition of a yield surface due to a hardening, changing the yield strength to f_y' according to following equation:

$$f_y' = f_y - \rho \tag{17}$$

Applying the kinematic hardening, the relation between to a plastic strain increment is made by kinematic hardening modulus - H_k:

$$\delta\rho_{ij} = H_k d\epsilon_{ij}^{pl} \tag{18}$$

4.2 Description of Parameters

All material parameters describing mechanical phenomena have to be considered depending on temperature and microstructural phase. Therefore the determination can be undertaken

by applying an experimental thermo-mechanical simulation (TMS). This approach consists of simulating a desired temperature-time regime purposing the metallurgical transformation to a definite phase. When the material of the specimen is completely transformed, the simulation stops and a characterization test is preformed. The procedure has to be repeated for different temperatures. Due to the instability of phases at certain temperatures, the experiments have to be preformed at high strain rates. For that reason the validity of parameters identified in such manner is not always assured for all strain rates. Besides that, the identification effort by experiments is relatively high. The most of mechanical material properties, such as Young's modulus, Poisson's ratio and yield strength can be identified by means of uniaxial tensile test. For the determination of kinematic hardening modulus cyclic loading tests have to be carried out. Thermal coefficient of expansion can be experimentally measured performing a dilatometer test. Furthermore, the material parameters describing the transformation plasticity behavior are also part of other constitutive relations and their experimental determination procedure have already been described in 3.3. Table 3 shows an overview of material parameters required for the description of mechanical behavior of welded steel material.

material parameter	unit	identification
Young's modulus - E	$\left[\frac{N}{mm^2}\right]$	TMS & tensile test, indirect method
Poisson's ratio - ν	$[-]$	TMS & tensile test, indirect method
yield strength - f_y	$[-]$	TMS & tensile test, indirect method
thermal coefficient of expansion - α^{th}	$[1/K]$	TMS & dylatometry, indirect method

Table 3: Overview of mechanical material parameters

5   RESULTS

The numerical calculation of residual stresses is based on mechanical description of material behavior by means of formulation of energy equilibrium state principles. An energy balance is drawn according to 1st fundamental theorem of thermodynamics which signifies the thermodynamic state in continuum due to its internal energy. The equality of thermal and mechanical energy applies. The FE calculations have been carried out by commercial software SYSWELD. The thermal and metallurgical calculation has been carried out in one step, taking into account their mutual interaction. The calculated temperature distribution as well as the temperature rate induces microstructural transformations. The free enthalpy dedicated for the microstructural process is influencing the thermal responses within the weld and HAZ. A numerical determination of residual stresses and distortion state has been carried out in a one way coupled mechanical substep. The generated transient temperature field caused by the heat source has been incorporated into the mechanical calculation as a load magnitude. Furthermore, calculated phase proportions in the workpiece during heating and cooling process influences the mechanical behavior. The influence of emerging mechanical responses on thermal and metallurgical behavior is neglected. The described FE approach is called a partly decoupled approach and it is shown in figure 8.
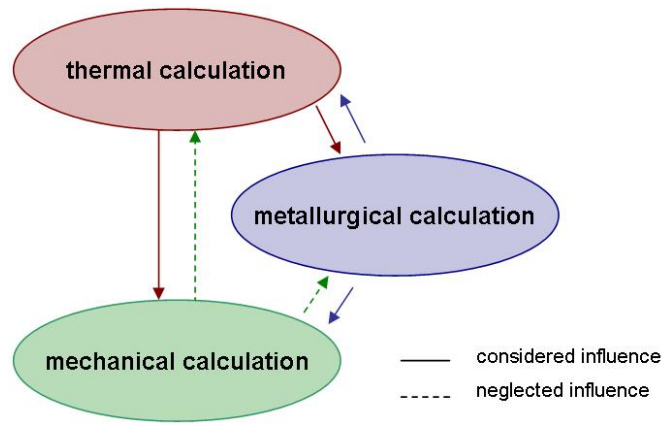
Figure 8: Partly decoupled FE approach

For example, a distribution of residual stresses in a butt welded joint of two 10 mm thin plates consisting of high-strength fine grained steel S460M has been calculated. The FE-Model is based on an experimental welding which has been preformed to verify the results of the numerical calculation. The joining technology of the MAG-welding has been simulated, applying the Goldak's heat source described in 2.2. Furthermore figure 9 shows the geometry of a weld pool and the temperature distribution within the welding connection. The comparison of temperature distribution in a cross section with the macro-examination specimen shows quantitatively good compliance of geometry of the weld and the HAZ.
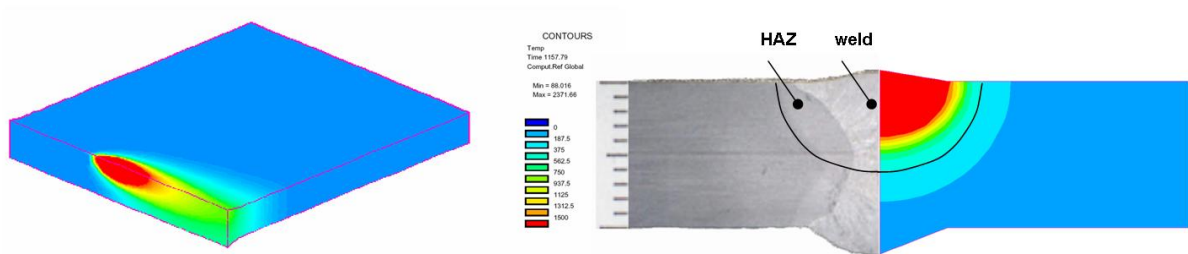

Figure 9: left: Temperature distribution due to heat source, right: Geometry of weld and HAZ vs. macro-examination specimen

The temperature distribution on local points of the specimen has been measured during the welding experiments by means of heat resistant thermocouples. The measured and calculated results, as seen in figure 10, show relatively good compliance.
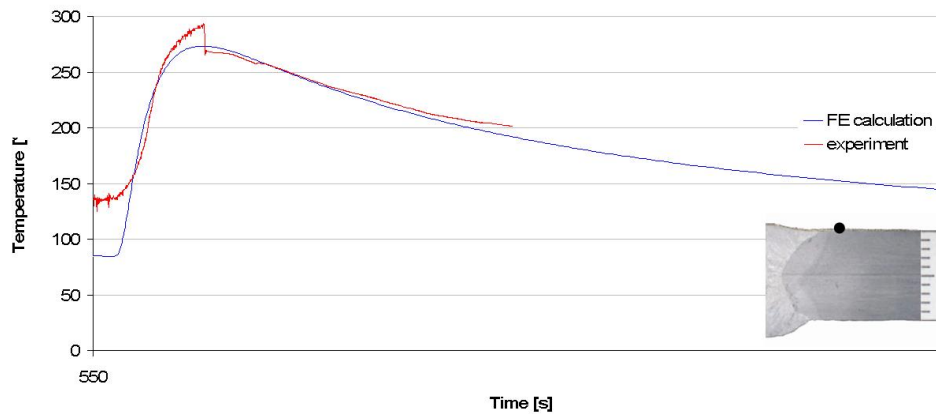
Figure 10: Comparison of measured and calculated thermal responses

Figure 11 shows the change of phase distributions of ferrite and martensite phase in the specimen with increasing distance from the weld. The results evidence the different metallurgical properties in the weld and the HAZ. Figure 11 signifies the typical increase of martensite phase in the HAZ which results in high strength and low ductility of this local area after welding. Further experimental investigations are necessary to quantitatively testify the calculated metallurgical responses.
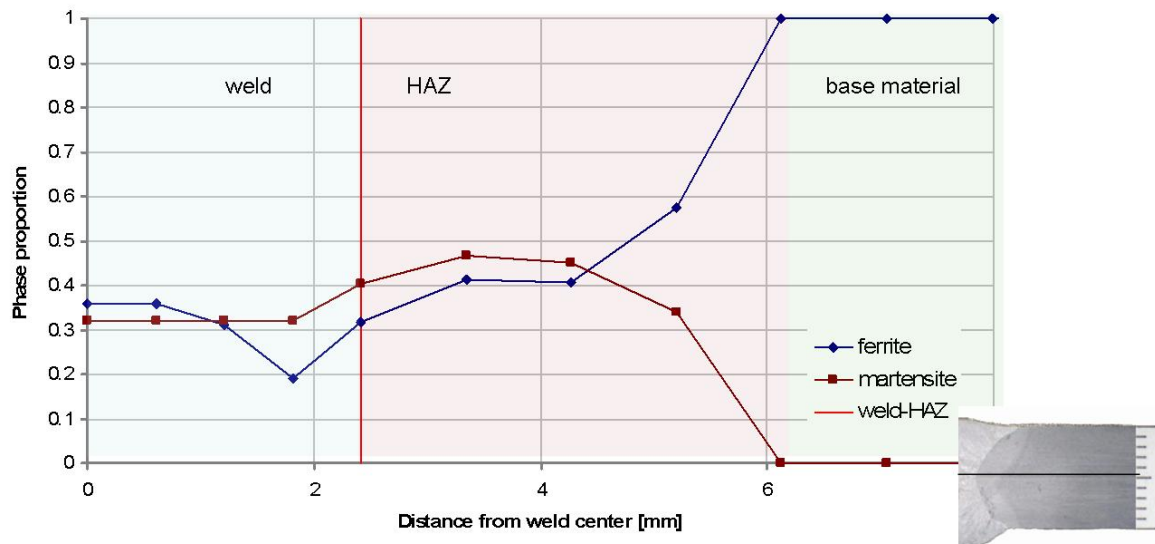

Figure 11: Distribution of ferrite and martensite phases within the workpiece

To demonstrate the influence of metallurgical phenomena on the mechanical responses, residual stresses have been calculated with and without the consideration of phase transfor-

14

mation. The calculation has been implemented on a two-dimensional FE-Model assuming a plane strain state. Results of transverse stresses of both calculations are illustrated in figure 12.
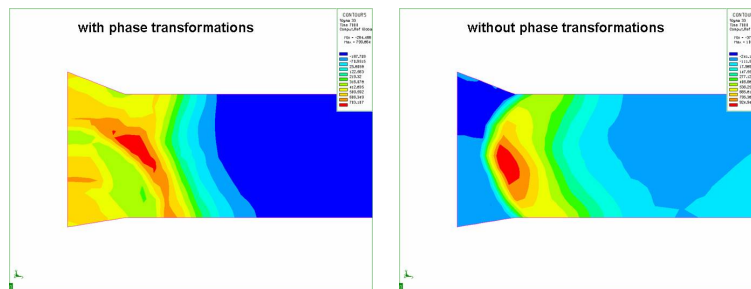

Figure 12: Influence of phase transformation on distribution of transverse residual stress

The application of plane strain state assumes a non-existence of strains in longitudinal direction (out of plane). This leads to an unrealistic supposition of constraints and to an overestimation of residual stress states in both calculations in figure 12. Nevertheless, their qualitative distribution can be compared, showing significant influence of microstructural transformation on mechanical responses in local areas of the welded joint. Residual stresses, calculated assuming the presented material phenomena in this paper, follow a macroscopic approach. Thus, the calculated stresses are residual stresses of 1st order. Besides that residual stresses of 2nd and 3rd order which develop in a grain size range and crystal size range, can be explicitly determined by modeling the material on the mesoscopic and microscopic scale.

6 CONCLUSIONS

The application of partly decoupled approach by means of continuum mechanics facilitates the calculation of structural responses due to welding. The numerical results demonstrate the ability of a qualitative prediction of welded connections. It has been shown that there is a wide array of material parameters which are affecting the thermal, metallurgical and mechanical behavior, and which have to be identified. The integration of local effects of a joint in structural analysis of steel constructions requires higher approaches towards quality. For that purpose further investigations are necessary to analyze the sensitivity of the models towards different material properties. The experimental determination of every material parameter is not possible due to the extraordinary laborious efforts needed. Besides that, experimentally identified parameters can be applied only for the tested steel quality for measured temperature-time regimes. For that reason alternative approaches for identification of material parameters, such as optimization strategies, have to be applied. After a definition of material parameters a quantitative prediction of welded connections will also be possible.

Numerical results show the effect of phase transformation, activated by welding process, on residual stress state. As these local phenomena occur in local areas in the range of crystal and grain sizes, the description of microscopic phenomena and their propagation on a macroscopic level due to approaches of homogenization might be expedient. Nevertheless, one should bear in mind, the increasing number of material parameters as well as the complexity of their experimental determination. Thus the microscopic approach should always be investigated under

the scope of ability and efficiency of a required prediction. Under certain circumstances a step backwards, adopting a phenomenological approach, also can be beneficial.

REFERENCES

[1] K.–J. Bathe, *Finite Elemente Methoden*. Springer Verlag, Berlin, 2002.

[2] H. Mang, G. Hofstetter, *Festigkeitslehre*. Springer Verlag, Wien, 2000.

[3] S. Roeren, *Klomplexitätsvariable Einflussgrößen für die bauteilbezogene Struktursimulation thermischer Fertigungsprozesse*. Diss., Thechnische Universität München 2007.

[4] U. Peil, M. Wichers, *Schweißen unter Betriebsbeanspruchung - Numerische und experimentelle Bestimmung des Temperaturfeldes beim Schweißen*. Stahlbau 74, **11**, 2005.

[5] C. Veneziano, M. Brand, M. Burdack, Y. Sguaizer, W. Pfeiffer, B. Urich and D. Siegele, *Numerische Simulation von Verug und Eigenspannungen geschweißter Komponeneten aus Al-Guss und Strangpressprofilen*. Project Report DVS-Nr. 9.032, Fraunhofer Institut IWM, 2006.

[6] D. Radaj, *Schweißprozesssimulation: Grundlagen und Anwendungen*. Fachbuchreihe Schweißtechnik no. 141, Verlag für Schweißen und Verwandte Verfahren, Düsseldorf, 1999.

[7] N. Schuster, V. G. Kolobrodov *Infrarotthermographie*. Wiley-VCH, 2004.

[8] A. N. Brink, *Einsatz der Impuls-Thermografie zur quantitativen zerstörungsfreien Prüfung im Bauwesen*. Diss., Thechnische Universität Berlin 2004.

[9] A. V. Kvasha, V. S. D'yachenko, *Effect of Grain Size on the Inhibition of Alpha and Gamma Transformation in Continuous Heating of Steel*. Journal of Metal Science and Heat Treatment, **30**, 1988.

[10] D. Roos, C. Groth, A. Junk, D. Brinkmann, *Optimierung und Sensitivitätsanalyse zur Parameteridentifikation in der numerischen Simulation der Gefügekinetik im Schweißprozess*. Conference Proceedings. 22nd CAD-FEM User's Meeting, Dresden, 2004.

[11] P. Pasquale, *Numerische Simulation schweißtechnischer Fertigungsschritte*. Diss., Thechnische Universität Karlsruhe, 2001.

[12] M. Wolff, M. Böhm, D. Helm, *Material Behavior of Steel Modeling of Complex Phenomena and Thermodynamic Consistency*. International Journal of Plasticity, **24**, 2008.

[13] M. Coret, S. Calloch, A. Combescure, *Experimental study of the phase transformation plasticity of 16MND5 low carbon steel induced by proportional and nonproportional biaxial loading paths*. European Journal of Mechanics A/Solids, **23**, 2004.